Forensic Science International 252 (2015) 11–21

Contents lists available at ScienceDirect

Forensic Science International

journal homepage: www.elsevier.com/locate/forsciint

Forensic analysis of explosions: Inverse calculation of the charge mass

M.M. van der Voort *, R.M.M. van Wees, S.D. Brouwer, M.J. van der Jagt-Deutekom, J. Verreault

TNO, Lange Kleiweg 137, 2280 AA Rijswijk, The Netherlands

ARTICLE INFO

Article history:
Received 30 January 2015
Received in revised form 8 April 2015
Accepted 10 April 2015
Available online 18 April 2015

Keywords:
Explosion
Forensic analysis
Blast
Debris
Damage
Statistical analysis

ABSTRACT

Forensic analysis of explosions consists of determining the point of origin, the explosive substance involved, and the charge mass. Within the EU FP7 project Hyperion, TNO developed the Inverse Explosion Analysis (TNO-IEA) tool to estimate the charge mass and point of origin based on observed damage around an explosion. In this paper, inverse models are presented based on two frequently occurring and reliable sources of information: window breakage and building damage. The models have been verified by applying them to the Enschede firework disaster and the Khobar tower attack. Furthermore, a statistical method has been developed to combine the various types of data, in order to determine an overall charge mass distribution.

In relatively open environments, like for the Enschede firework disaster, the models generate realistic charge masses that are consistent with values found in forensic literature. The spread predicted by the IEA tool is however larger than presented in the literature for these specific cases. This is also realistic due to the large inherent uncertainties in a forensic analysis. The IEA-models give a reasonable first order estimate of the charge mass in a densely built urban environment, such as for the Khobar tower attack. Due to blast shielding effects which are not taken into account in the IEA tool, this is usually an under prediction. To obtain more accurate predictions, the application of Computational Fluid Dynamics (CFD) simulations is advised.

The TNO IEA tool gives unique possibilities to inversely calculate the TNT equivalent charge mass based on a large variety of explosion effects and observations. The IEA tool enables forensic analysts, also those who are not experts on explosion effects, to perform an analysis with a largely reduced effort.

1. Introduction

Forensic analysis of explosions consists of determining the point of origin, the explosive substance involved, and the charge mass. In the case of deliberate explosions, this information is desirable to trace production facilities of illicit materials and eventually the perpetrator. In the case of accidental explosions, this information is important to identify the cause of the explosion, and to develop appropriate safety measures.

Although literature on post blast forensic investigation [1–3] contains a wealth of information, the descriptions are mainly qualitative. Furthermore, the focus is on collecting explosive residues and possible remains of a bomb. The current paper presents a quantitative method to estimate the TNT equivalent charge mass and point of origin based on observed damage around the explosion.

Two frequently occurring and reliable sources of information are observations on window breakage and building damage [11–14]. Also the size of a crater, fireball diameter, break-up of an enclosure in which the bomb is located, and debris throw of the enclosure may provide valuable information. For the various phenomena we have developed inverse models, which give an estimate of the charge mass (including an error) typically as a function of damage level and distance. These models have been implemented in the TNO Inverse Explosion Analysis (IEA) tool, which was developed for on-site application by a forensic analyst [21]. The tool enables the user to define evidence locations based on OpenStreetMaps, and add specific damage information. An example is given in Fig. 1 for the entry of window breakage evidence.

Terrorist bombing attacks and accidental explosions are often humanitarian disasters. Although the number of fatalities and injured people may exhibit a correlation with charge mass, we did not use this information for inverse calculations. The reason is the large inherent uncertainty in the location of people during the explosion, their protection and vulnerability.

* Corresponding author. Tel.: +31 888 66 12 88.
E-mail address: martijn.vandervoort@tno.nl (M.M. van der Voort).

http://dx.doi.org/10.1016/j.forsciint.2015.04.014
0379-0738/

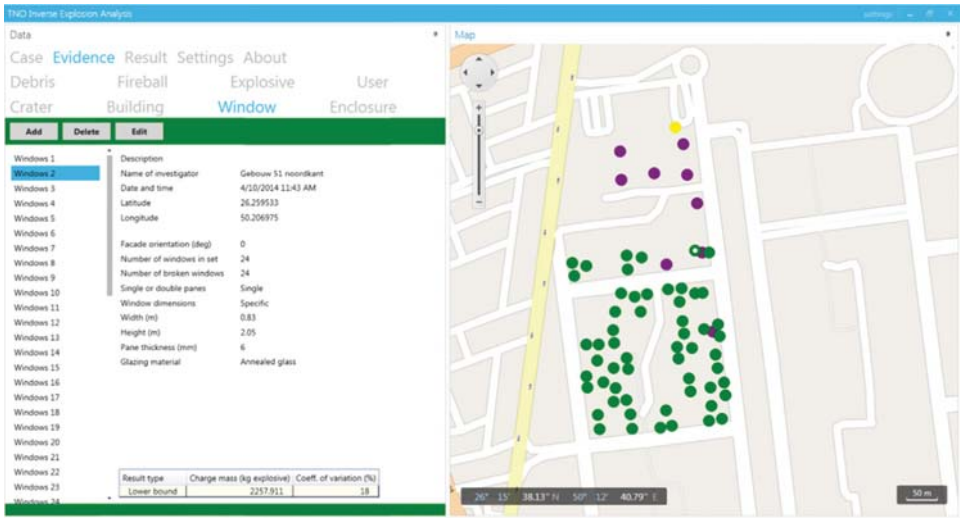

Fig. 1. Screenshot of the TNO IEA tool. Evidence tab with window breakage evidence entry [21].

The application of the method is limited to explosives which can be reasonably well represented by a TNT equivalency based on blast. These are typically high explosives with a large velocity of detonation and brisance such as TNT, RDX, and PETN. The concept of TNT equivalency has its limitations: different values can be found in the literature depending on whether it is based on overpressure or impulse, and the TNT equivalency can also depend on distance. For improvised explosives, including secondary combustion, and fireworks these deviations typically increase. The error made with the TNT equivalency should always be regarded together with other uncertainties, and as will become clear from the paper, these can be substantial. Gas and dust explosions should not be analysed with the IEA tool.

The inverse calculations lead to a set of charge mass estimates with varying reliability. Furthermore, some estimates give just a lower or upper bound. A statistical method has been developed to combine the various types of data, and to determine an overall charge mass distribution. This method is presented in Section 2.

In order to limit the scope of the paper, we focus in Sections 3 and 4 on the inverse models that have been developed for building damage and window breakage. These models are verified by their application to the Enschede firework disaster in 2000 [12–14] and the Khobar tower attack in 1996 [15–18] respectively. The blast shielding effect in a densely built urban area is not taken into account in the relatively simple inverse models. This effect is illustrated with Computational Fluid Dynamics (CFD) simulations of the blast propagation in the Khobar tower geometry, and modelling of the window response with a Single Degree of Freedom (SDOF) model. In Section 5 conclusions are presented.

2. Combining multiple charge mass predictions

The post blast evidence leads, together with an assumed point of origin, to multiple charge mass predictions including an error estimate. The charge mass predictions can be of three types. In the first type, the observed damage can be translated to a prediction of the blast strength, which can be translated to a single value prediction of the charge mass. However, many objects, e.g. windows, are either undamaged or completely broken. When such an object is broken, the result is a lower bound of the charge mass, while an undamaged object leads to an upper bound prediction. Practical considerations like the maximum load capacity of the vehicle used to carry the bomb may also lead to upper bounds. Single valued charge mass predictions are the most reliable type of data. Examples are façades where a part of the windows failed or where the building was damaged at an intermediate level.

In this section we present a method to determine an overall charge mass distribution based on the data types described above. The method is an extension of the least squares method.

2.1. The least squares method for single valued data

For a collection of N single valued charge mass predictions M_i, the sum of squared residuals R is:

$$R(M) = \sum_{i=1}^{N} (M_i - M)^2 \tag{1}$$

The average charge mass is defined as the M at which R has a minimum, i.e. where $dR/dM = 0$. This requirement leads directly to the arithmetic mean. When error estimates are available for each of the predictions, the charge masses can be characterized by their mean charge mass μ_i, and standard deviation σ_i : $M_i = (\mu_i, \sigma_i)$. In order to account for the error, the weighted sum of squared residuals can be defined as follows:

$$wR(M) = \sum_{i=1}^{N} \frac{1}{\sigma_i^2} (\mu_i - M)^2 \tag{2}$$

Minimization of this function shifts the average M towards data points with a smaller standard deviation. This is illustrated with an example in Fig. 2.

The resulting average charge mass and standard deviation of the average are given by:

$$M_{av} = \frac{\sum_{i=1}^{N} \frac{1}{\sigma_i^2} \cdot \mu_i}{\sum_{i=1}^{N} \frac{1}{\sigma_i^2}} \tag{3}$$

$$\sigma_M = \sqrt{\frac{\sum_{i=1}^{N} \frac{1}{\sigma_i^2} \cdot (\sigma_i^2 + \mu_i^2)}{\sum_{i=1}^{N} \frac{1}{\sigma_i^2}} - M_{av}^2} \tag{4}$$

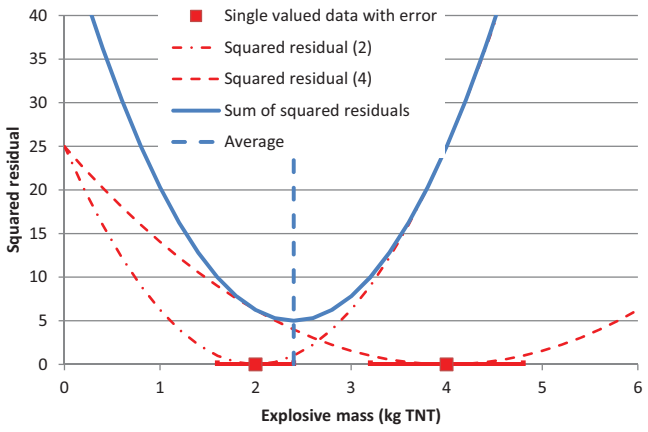

Fig. 2. Sum of squared residuals calculated for two single values at 2 and 4 kg with an error.

2.2. The least squares method for lower and upper bounds

We have extended the least squares method for lower and upper bounds. The concept is that for lower bounds, residuals are only taken into account for charge masses M below the boundary M_i, while for upper bounds, residuals are only taken into account above the boundary. Although this concept seems quite obvious and straightforward, no description was found in the literature. The above suggests that Eq. (1) can be extended with the following residuals for lower (LB) and upper (UB) bound data:

$$R_{LB}(M) = \begin{cases} (M_i - M)^2 & if \quad M < M_i \\ 0 & otherwise \end{cases} \tag{5}$$

$$R_{UB}(M) = \begin{cases} (M_i - M)^2 & if \quad M > M_i \\ 0 & otherwise \end{cases} \tag{6}$$

The squared residuals from single values, lower and upper bounds are illustrated with an example in Fig. 3. In this particular example the lower and upper bound do not influence the average.

It is less straightforward how to include error estimates to squared residuals for the lower and upper bounds. To achieve this in a mathematically sound fashion, all possible locations of the boundary must be integrated. Additionally, the residuals must be weighted with the square of the standard deviation like in Eq. (2):

$$wR(M, \mu_i, \sigma_i) = \frac{1}{\sigma_i^2} \cdot \int_{-\infty}^{\infty} f(M, \mu_i, \sigma_i, M_i) \cdot dM_i \tag{7}$$

For lower bounds:

$$f(M, \mu_i, \sigma_i, M_i) = \frac{1}{\sigma_i \cdot \sqrt{2 \cdot \pi}} \cdot e^{-\frac{1}{2} \cdot \left(\frac{M_i - \mu_i}{\sigma_i}\right)^2} \cdot (M - M_i)^2 \text{ if } M < M_i$$
$$f(M, \mu_i, \sigma_i, M_i) = 0_i \quad \text{otherwise} \tag{8}$$

For upper bounds:

$$f(M, \mu_i, \sigma_i, M_i) = \frac{1}{\sigma_i \cdot \sqrt{2 \cdot \pi}} \cdot e^{-\frac{1}{2} \cdot \left(\frac{M_i - \mu_i}{\sigma_i}\right)^2} \cdot (M - M_i)^2 \; if \; M > M_i$$
$$f(M, \mu_i, \sigma_i, M_i) = 0_i \quad otherwise \tag{9}$$

The difference between a lower bound with and without an error estimate is shown in Fig. 4. The effect of the error is that the residual function has non-zero values above the lower bound. For upper bounds an analogous result can be obtained.

In order to get the complete residual function, the weighted residual contributions for single values (Eq. (2)), lower bounds (Eqs. (7) and (8)) and upper bounds (Eq. (7) and (8)) have to be summed. Minimizing the resulting equation will then yield the average charge mass.

2.3. Correction for lognormal distribution

In forensic analysis of explosions the standard deviation of the charge mass, and hence the coefficient of variation, is often quite large. Together with the assumption of a symmetric distribution, the probability of having a negative charge mass may be significant. Choosing for a lognormal distribution, which is only defined for positive charge masses, avoids this unphysical phenomenon. In addition most models for blast damage are more naturally expressed on a logarithmic scale.

For this reason the procedure described above is not applied to the charge mass, but to the natural logarithm of the charge mass. The resulting average charge mass should therefore be interpreted as a geometric mean, rather than an arithmetic mean.

2.4. Finding the point of origin

As mentioned at the start of Section 2, the charge mass predictions depend on an assumed point of origin. This point

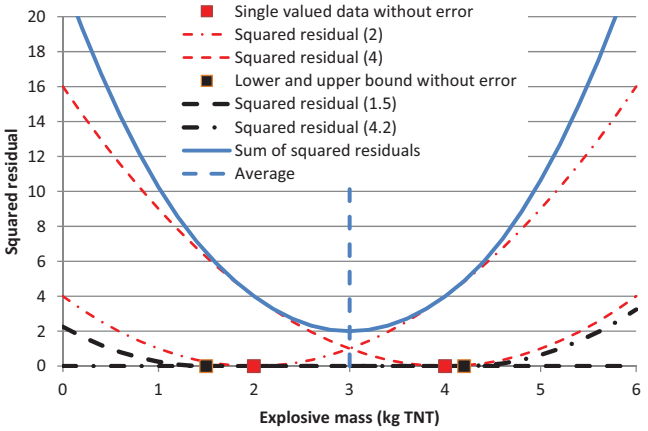

Fig. 3. Sum of squared residuals calculated for two single values at 2 and 4 kg, a lower bound at 1.5 kg and an upper bound at 4.2 kg, all without error.

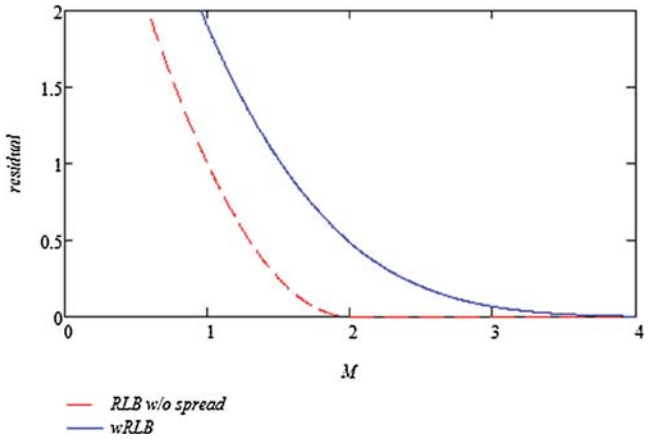

Fig. 4. Squared residual of a lower bound without an error (R_{LB} w/o spread) and weighted squared residual of a lower bound with an error (wR_{LB}), for $M_i = \mu_i = 2$ and $\sigma_i = 1$.

Table 1
Housing damage levels and *RB* ratio from Gilbert, Lees and Scilly [6].

Damage level	*RB* ratio	Description
A	0.675	Houses completely demolished, i.e. with over 75% of the external brickwork demolished.
B	1.00	Houses so badly damaged that they are beyond repair and must be demolished when opportunity arises. Property is included in this category if 50–75% of the external brickwork is destroyed, or in the case of less severe destruction, the remaining walls have gaping cracks rendering them unsafe.
C_b	1.74	Houses which are rendered uninhabitable by serious damage, and need repairs so extensive that they must be postponed until after the war. Examples of damage resulting in such conditions include partial or total collapse of roof structures, partial demolition of one or two external walls up to 25% of the whole, and severe damage to load-bearing partitions necessitating demolition and replacement.
C_a	3.0	Houses that are rendered uninhabitable, but can be repaired reasonably quickly under wartime conditions, the damage sustained not exceeding minor structural damage, and partitions and joinery wrenched from fixings.
D	6.0	Houses requiring repairs to remedy serious inconveniences, but remaining habitable. Houses in this category may have sustained damage to ceilings and tiling, battens and roof coverings, and minor fragmentation effects on walls and window glazing. Cases in which the only damage amounts to broken glass in less than 10% of the windows are not included.

determines the distances and orientations with respect to the other evidence locations. In many cases the point of origin will be clear, due to the presence of a crater or due to fragment patterns. Uncertainty about the point of origin is possible, especially for relatively small explosive charges or in case of a dense subsoil. Also due to a post blast fire, the point of origin may be obscured. In these cases the assumed point of origin will have to be varied to find an optimum. It is to be expected that the spread in the charge mass has a minimum value for the correct point of origin.

3. Building damage evidence

In this section, we describe an existing model for the prediction of blast damage to brick buildings. Next, we will derive the inverse form of the model and apply it to the Enschede firework disaster.

3.1. Model description

During the World War II, damage from German bombings on England was analysed by E.B. Philip. She derived functions for the average damage radius for various levels of damage to typical U.K. houses (i.e. brick terraced dwellings). These were later declassified and published by Jarrett [7]. The original description gives only a short presentation of the building damage model. Stone and Henderson [5] gave an extensive description of the model, its derivation and its background. Scilly and High [4] and Gilbert, Lees and Scilly [6] evaluated Philip's work and rewrote the equation into a form that uses the TNT-equivalent charge mass.

Gilbert, Lees and Scilly [6] published the following equation for the Average Circle Radius (ACR) as a function of the TNT equivalent charge mass (M):

$$\mathrm{ACR} = \frac{RB \cdot k_{\mathrm{ACR}} \cdot M^{1/3}}{\left[1 + \left(\frac{M_{\mathrm{ACR}}}{M}\right)^2\right]^{1/6}} \tag{10}$$

In this equation, *RB* is the ratio of the ACR for a particular damage level to the ACR of damage level B. In Table 1, a description of the various damage levels is given, as well as the corresponding *RB* values. Eq. (10) contains the following constants: k_{ACR} = 7.1 m/kg$^{1/3}$, M_{ACR} = 3175 kg.

This work is mainly based on data from WW II air raids, so the criteria apply to the housing of that period: 1900–1940 style brick houses, single leaf wall, wooden floors and roof, 2–4 storeys high. It should be noted that the orientation of a building is not a variable in the model.

3.2. Derivation of an inverse model

Building damage evidence consists of an observation of the damage level and the distance from the building to the explosion. For forensic analysis we are therefore interested in the inverse form of Eq. (10), expressing the TNT equivalent charge mass as a function of damage level and range. Mathematically the determination of the inverse form is quite straightforward. However, we should realize that in the inverse form some variables take on a different meaning and for clarity they are replaced by new variables. The ACR is replaced by the observed distance from the centre of the explosion to the centre of the building (r_{obs}). The ratio *RB* is replaced by RB_{obs}, the *RB* ratio for the observed damage level. This gives:

$$M = \frac{1}{2} \cdot \sqrt{2} \cdot \sqrt{\left(\frac{r_{obs}}{RB_{obs} \cdot k_{ACR}}\right)^3 \cdot \left[\left(\frac{r_{obs}}{RB_{obs} \cdot k_{ACR}}\right)^3 + \sqrt{\left(\frac{r_{obs}}{RB_{obs} \cdot k_{ACR}}\right)^6 + 4 \cdot M_{ACR}^2}\right]} \tag{11}$$

In order to use this equation to determine a TNT equivalent charge mass including an error estimate, we have reanalysed the data from the WW II. The original definition of the ACR of damage level B is: "a circle drawn around the centre of an explosion which damages dwelling houses such that there are as many damaged to the level of damage or greater outside the circle as there are of less than level B damaged inside the circle" [5]. This is illustrated in Fig. 5 with one of the original bomb damage plots. The blue houses

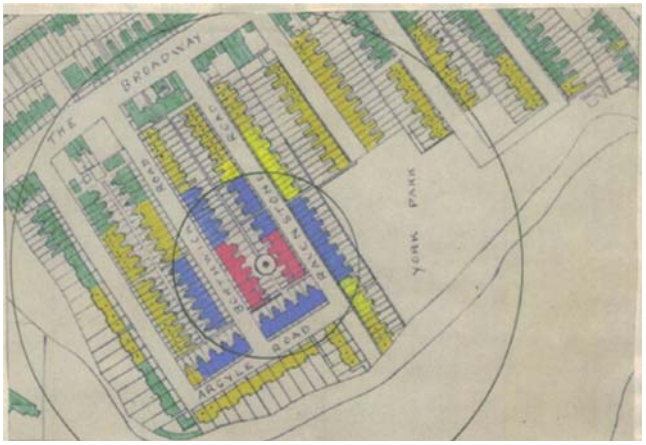

Fig. 5. Typical bomb damage plot from Stone and Henderson [5] for a 2500 kg light alloy cased bomb in a moderately built up area. Damage level A (red), B (blue), C (yellow), and D (green). (For interpretation of the references to color in this figure legend, the reader is referred to the web version of the article.)

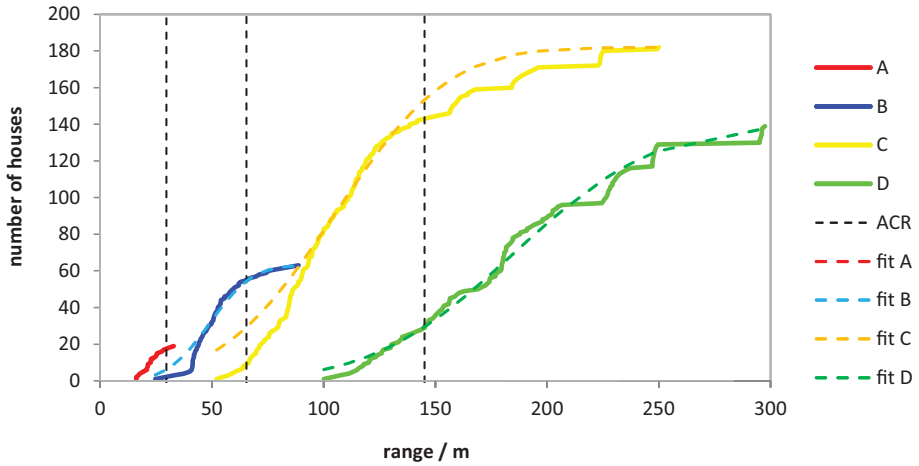

Fig. 6. Cumulative distribution for each damage category as a function of range together with data-fitted curves.

have damage level B, the yellow houses C. The inner circle is the ACR for damage level B. The number of blue houses outside this circle is equal to the number of yellow houses inside the circle.

From the data in the bomb damage plot, cumulative distributions can be constructed for the various damage levels as in Fig. 6. The figure shows that for the various damage levels the ACR does not correspond to the distance where 50% of the houses are damaged. The distributions could be reasonably well fitted with cumulative normal functions. It appeared that the mean of each distribution falls halfway between the ACRs for the relevant damage levels, e.g. the mean value of damage level B lies halfway between the ACR of damage levels A and B. Furthermore, the coefficient of variation appeared to be about 30% for all damage levels. Available data on damage level C was not separated into C_a and C_b as in Table 1. The same logic as described above was followed to obtain results from C_a and C_b separately.

The original definition of damage level D has been extended to houses with less damage and undamaged houses. The reason is that in a forensic analysis the presence of the undamaged houses provides information as well, and is therefore desirable to include. Table 2 gives the resulting parameter values and also indicates whether the charge mass is a lower bound, single valued, or an upper bound.

A mean TNT equivalent charge mass (μ) can now be determined by applying Eq. 11 with the appropriate mean value for RB_{obs} from Table 2. The standard deviation of the charge mass (σ) is determined using the standard deviation in RB_{obs} (σ_{RBobs}):

$$\sigma \cong \frac{M(RB_{obs} + \sigma_{RBobs}) - M(RB_{obs} - \sigma_{RBobs})}{2} \quad (12)$$

In order to verify the inverse building damage model, it has been applied to the Enschede fireworks disaster.

A major fireworks accident occurred at S.E. Fireworks in Enschede, The Netherlands, on May 13, 2000. In addition to the destruction of a complete residential area, there were 21 deaths and 947 wounded. The events started with a relatively small explosion in a container, followed by an explosion in seven pre-fab storage facilities (so-called Mavo boxes). The final explosion in reinforced concrete storage cell C11 was the largest. Evidence collected by Weerheijm [12–14] consisted of data on building damage, window breakage, debris and the diameter of the fireball.

The current validation focuses on the third and largest explosion, and on the observed building damage only. The Enschede residential area consisted of brick walled dwellings that resemble the UK housing to a reasonable extent. The observed building damage is displayed in Fig. 7.

Eqs. (11) and (12) have been applied to a total of 184 building damage observations. The resulting charge mass predictions are plotted as a function of range in Fig. 8. Note that upper bound data are shown with a (semi-)infinite lower error bar, while the lower bound data are shown with a (semi-) infinite upper error bar. A striking feature is the saw tooth pattern which is caused by the discrete damage levels. Within each 'tooth' are buildings classified with the same damage level, but at various ranges.

When all data is combined using the procedure described in Section 2, we obtain a charge mass distribution with a mean charge mass of 3,461 kg, and a large coefficient of variation of 124%. Charge masses between 1315 kg and 9107 kg are within one standard deviation from the average. These results are consistent with Spence, et al. [15], where a range of charge masses from 2330 to 7050 kg was reported based on all damage categories. In this reference, it was also concluded that a charge mass between 3750 and 5800 kg, based on damage category C_b only, is most realistic. This last interval is probably too narrow.

Table 2
Values for the mean and standard deviation of RB_{obs} for the various building damage levels. The result type of the charge mass is also indicated.

Damage level	RB_{obs} Mean	RB_{obs} Standard deviation	Result type (charge mass)
A	0.506	0.15	Lower bound
B	0.838	0.25	Single valued
C_b	1.37	0.41	Single valued
C_a	2.37	0.71	Single valued
C	2.00	0.6	Single valued
D	4.5	1.35	Upper bound

4. Window breakage evidence

In this section, we describe an existing model for the prediction of window breakage. Next, we will derive the inverse form of the model and apply it to the Khobar tower attack.

4.1. Model description

A relatively simple existing model for the prediction of window breakage starts with an explosion on a surface, a so-called hemispherical surface burst. A blast wave can be characterized by its peak overpressure (P) and impulse (i); the area below the positive phase of the overpressure-time profile. While the blast wave propagates away from the explosion center, its peak overpressure and impulse decay with distance. A semi-empirical relation for the decay of the blast wave is given by Kingery and

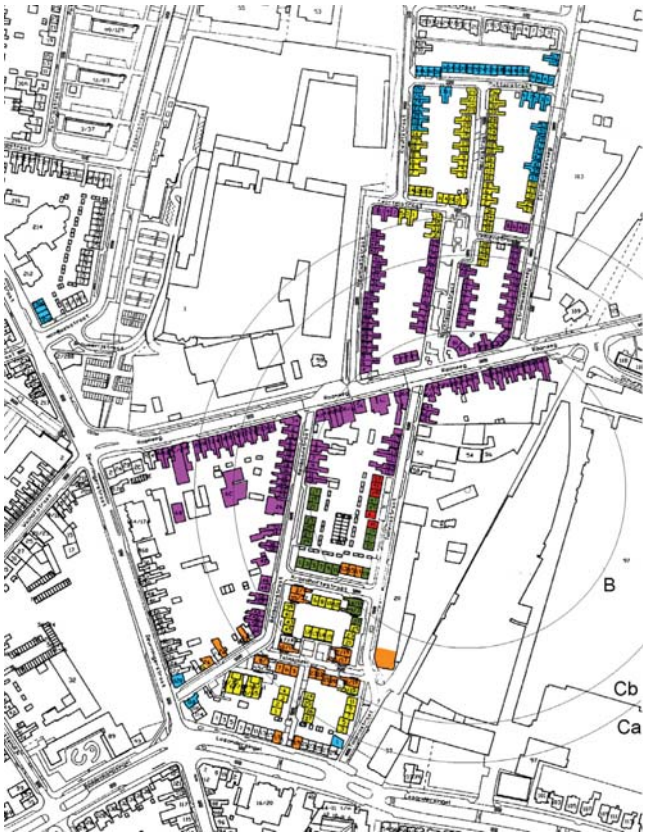

Fig. 7. Map of buildings that were damaged after the Enschede firework disaster. The buildings that are not coloured have very limited or no damage. Damage categories are indicated with colours: red (A), green (B), orange (C_b), yellow (C_a) and blue (D). Purple buildings are destroyed by fire and can therefore not be used as evidence. (For interpretation of the references to color in this figure legend, the reader is referred to the web version of the article.)

Bulmash [9,20]. The blast wave will interact with infrastructure, and exert a force load onto the façades of buildings. In the current simple model, we distinguish between two extreme cases. Façades oriented parallel to the blast wave propagation direction will receive a side-on blast load. Façades facing the explosion will be loaded with a higher reflected blast load. Note that while the building damage model described in Section 3 did not explicitly take into account the orientation of a building, the model for window breakage does take this into account, since we are now considering specific façades.

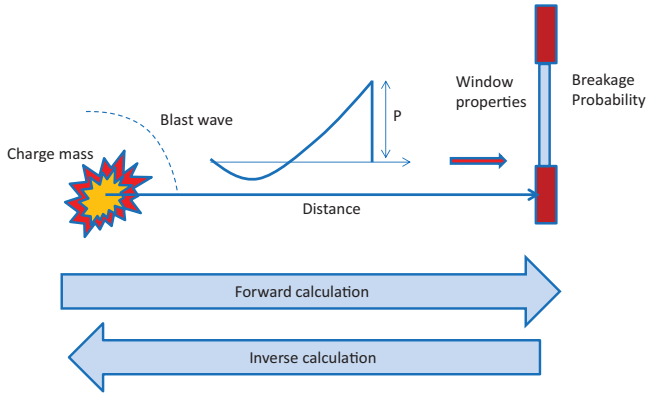

Fig. 9. Window breakage: forward and inverse calculation.

The resistance of windows to a dynamic pressure load depends on the size and thickness of the window panes, and the type of glazing. This may vary from single or double annealed glazing to tempered, laminated or wired glass. TM5-1300 [8] provides a method to calculate the dynamic resistance based on the window properties. The dynamic resistance is expressed in a so called *P–i* diagram; this is a curve that gives all combinations of the peak overpressure and impulse of a blast load that will result in the same breakage probability.

The above described model gives the probability of window breakage as a function of the TNT equivalent charge mass, range, façade orientation, and window properties. An overview is given in Fig. 9.

4.2. Derivation of an inverse model

Window breakage evidence consists of an observation of the number of broken windows in a façade, the façade orientation, the

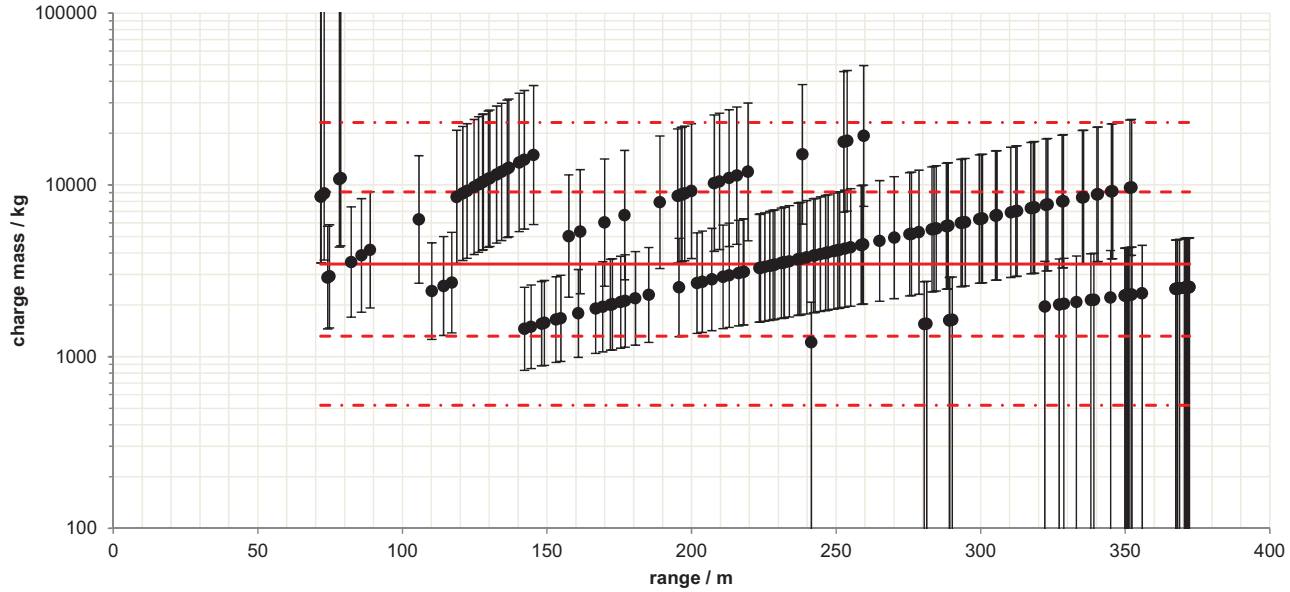

Fig. 8. Charge mass as a function of range. The red lines indicate the mean, plus and minus one standard deviation, and the 95% confidence limits. (For interpretation of the references to color in this figure legend, the reader is referred to the web version of the article.)

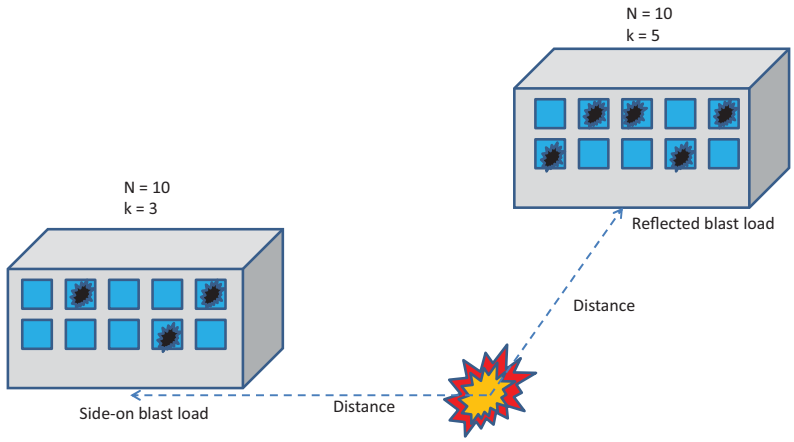

Fig. 10. Two examples of window breakage.

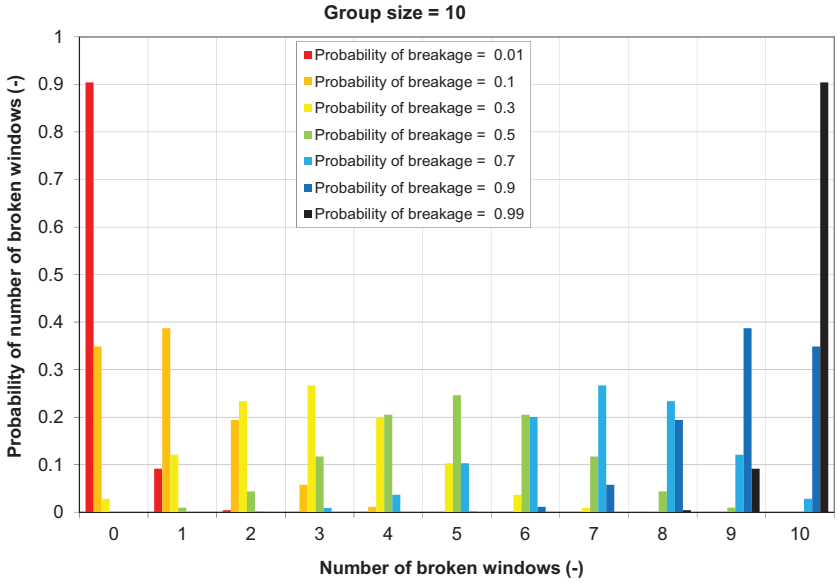

Fig. 11. Binomial distribution for different breakage probabilities and $N = 10$.

window properties, and the range. It is important to verify whether windows were not already broken before the explosion took place, and whether windows failed due to the blast wave, and not due to other explosion effects (e.g. impacting debris and fragments).

For forensic analysis, we are interested in an inverse form of the model described in Section 4.1. As a starting point, we calculate a representative range of breakage probabilities for a façade. We consider a group of N identical windows, of which k are broken. Two examples are shown in Fig. 10.

A first estimate for the probability of window breakage is:

$$P_{break} \approx \frac{k}{N} \tag{13}$$

Therefore, the most obvious thing to do would be to inversely calculate the charge mass which would generate exactly this probability of window breakage. In addition to this supposed mean value for the charge mass, an error estimate is needed. Note that the number of broken windows k follows a binomial distribution [10]:

$$P(k) = \frac{N!}{k! \cdot (N-k)!} \cdot P_{break}^{k} \cdot (1 - P_{break})^{N-k} \tag{14}$$

With: N, total number of windows; k, Number of broken windows; $P(k)$, The probability of finding k broken out of N windows; P_{break} The probability of breakage.

This distribution is plotted in Fig. 11 for $N = 10$ and for a number of breakage probabilities.

The distribution for a breakage probability of, for example, 0.5 (green) peaks at 5 broken windows out of 10. The figure shows, however, that 5 broken windows are also very well possible for a breakage probability of 0.3 (yellow) and 0.7 (light blue). Consistent formulas to calculate a relevant minimum, mean and maximum breakage probability are required. For this purpose, the inverse form of the binomial distribution is needed, i.e. $P_{break}(k)$ instead of $P(k)$. Although an analytical expression is not available, several approximations exist. The equations from Agresti-Coull [10] give the minimum, mean and maximum (breakage) probability for a given confidence level. The result for a group size of $N = 10$ with a confidence level of 1 standard deviation, is shown in Fig. 12. A striking feature in this figure is that Eq. (13) is exactly valid only for a breakage probability of 0.5. For smaller or larger breakage probability, a deviation occurs.

The minimum, mean and maximum breakage probability are now used to inversely calculate the charge mass and give an error

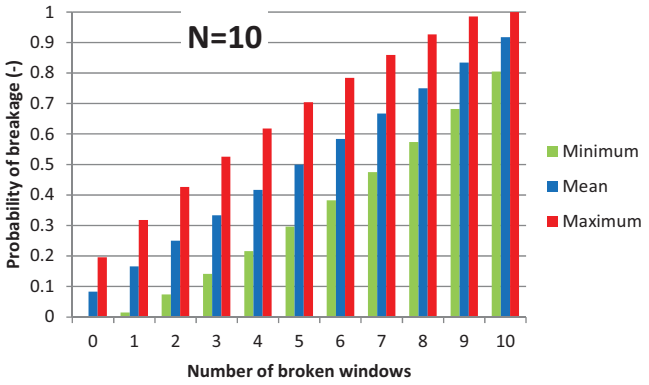

Fig. 12. Minimum, mean and maximum probability of window breakage for a group size of $N = 10$.

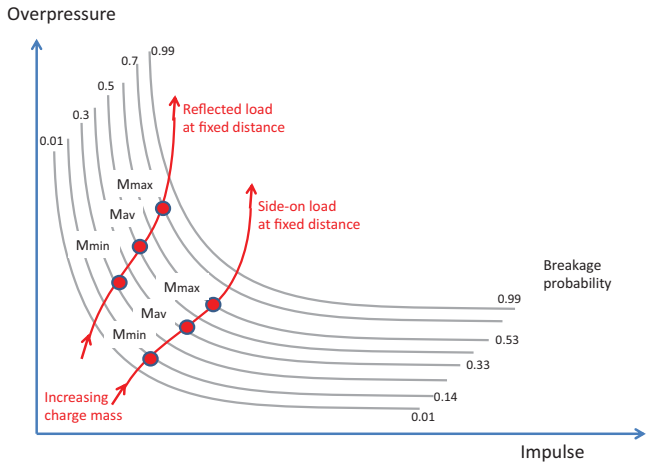

Fig. 13. Schematic *P–i* curves for glazing together with load curves for a fixed distance and varying charge mass. Probabilities have been selected for the two cases outlined in Fig. 10, and based on Fig. 12.

estimate. In Section 4.1, it was mentioned that *P–i* curves are available for given window properties and breakage probability. These curves are shown schematically in Fig. 13 for probabilities relevant for the case outlined in Fig. 10. The figure also shows load curves for a fixed distance (in a forensic analysis the distance is known), and increasing charge mass. The intersections between the *P–i* curves and the load curves are resolved by an iterative calculation procedure and yield the desired range of charge masses.

4.3. Application to the Khobar tower attack

On June 25, 1996, a terrorist's truck bomb exploded at the Khobar Towers housing compound in Dhahran, Saudi Arabia, killing 19 people and wounding 555 [15–18]. The force of the explosion was so great that it heavily damaged and destroyed high rise apartment buildings, shattered numerous windows and left a massive crater in the ground, Fig. 14.

The current validation considers window breakage only. The windows involved were two fixed glass façade panels and one sliding door (also called patio door) for each apartment. Window properties were not available, but have been estimated based on publicly available photographs to be single annealed 6 mm glazing windows with dimensions of 2.05 by 0.83 m. The observed window breakage at the Khobar tower compound is displayed in Fig. 15. The various façades contained either 24 or 12 windows.

The inverse model presented in Section 4.2 has been applied to a total of 57 sets of windows. The resulting charge mass predictions are plotted as a function of range in Fig. 16. Note that upper bound data are shown with a (semi-)infinite lower error bar, while the lower bound data are shown with a (semi-) infinite upper error bar.

When all data is combined using the procedure described in Section 2, a charge mass distribution with a mean of 5658 kg, and a coefficient of variation of 70% is obtained. Charge masses between 3019 kg and 10,602 kg are within one standard deviation from the average. This range of charge masses is significantly smaller than published by DSWA [17]. They reported a charge mass of 30,000 lbs or 13,600 kg based on window breakage.

4.4. Detailed analysis of the Khobar tower attack

The observed difference in Section 4.3 may be caused by the fact that DSWA based their findings on a detailed (not publicly available) analysis taking into account blast shielding effects. These effects are not addressed in the developed inverse model. In

Fig. 14. Overview of the Khobar Towers compound in Dhahran, Saudi Arabia, 1996.

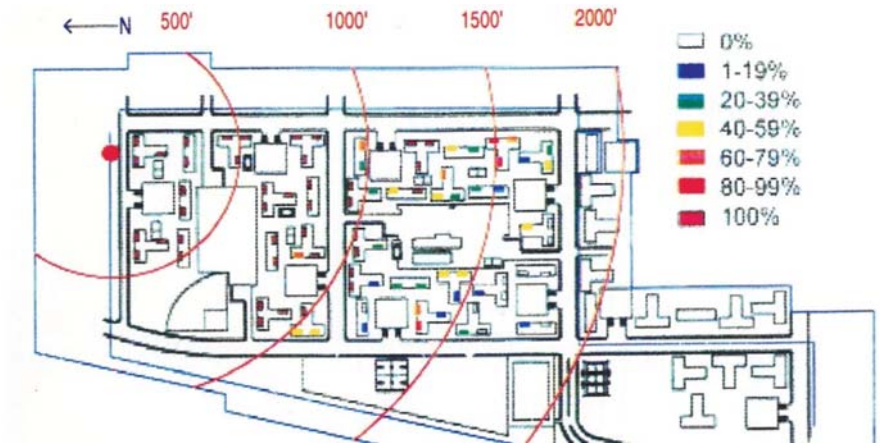

Fig. 15. Patio door glass breakage at the Khobar tower compound [18].

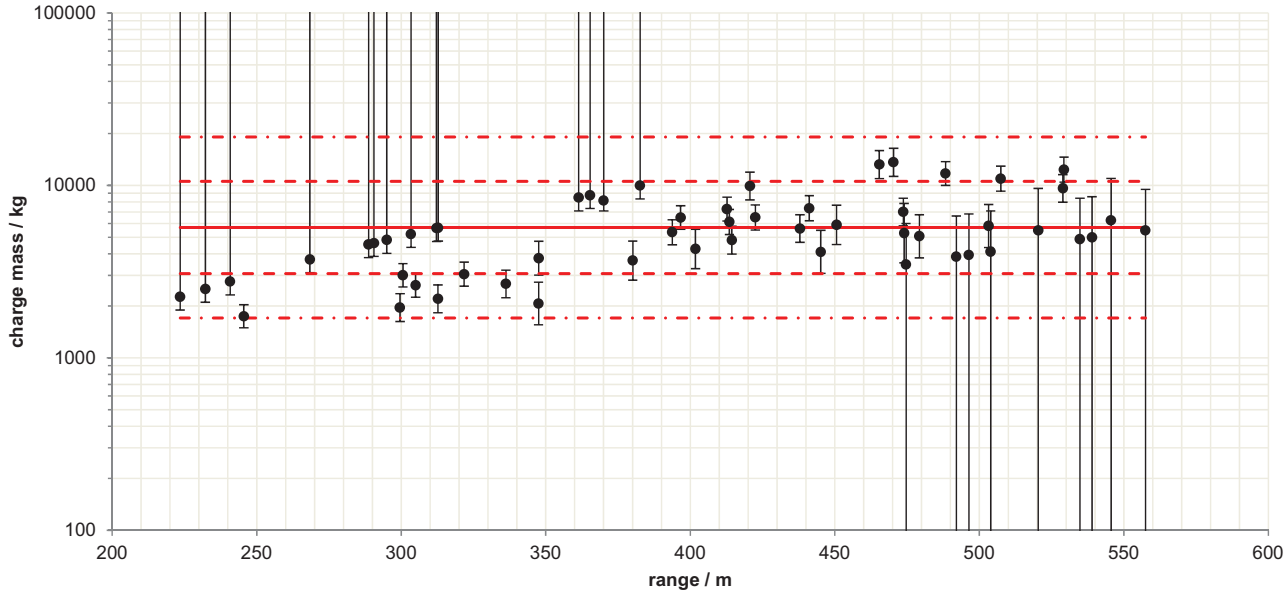

Fig. 16. Charge mass as a function of range. The red lines indicate the mean, standard deviation limits, and the 95% confidence limits. (For interpretation of the references to color in this figure legend, the reader is referred to the web version of the article.)

order to investigate this hypothesis, the blast propagation through the Khobar tower geometry was simulated with Autodyn [19].

In this section, two simulations are presented; one with a charge mass of 5436 kg (as predicted by the inverse model), and 13,600 kg (as published by DSWA). In both simulations, overpressure profiles have been recorded on various building façades. These profiles constitute inputs to a Single Degree of Freedom (SDOF) model to determine the window response and breakage probability. The breakage probability is then compared to the observed damage to assess the plausibility of the assumed charge mass.

The simulation setup is displayed in Fig. 17 showing the bomb location, the layout of the buildings and the location of the pressure gauges. One gauge is assigned per apartment. Note that the building closest to the bomb location is omitted from the simulation due to numerical difficulties. As a result the pressure load on the other buildings is slightly overestimated.

Initialization of the simulation is performed in a one-dimensional (1D) grid using spherical coordinates. This simulation is stopped slightly before the blast reaches the first building, which is approximately 80 m from the bomb location. A cell size of 2 mm is used for the 1D simulation to accurately resolve the blast profile. The flow field is then mapped from the 1D simulation into a 3D numerical domain as shown in Fig. 17. The cell size of the numerical domain is approximately 1.2 m for a total of approximately 28 million cells (the domain size is 550 m × 400 m × 225 m).

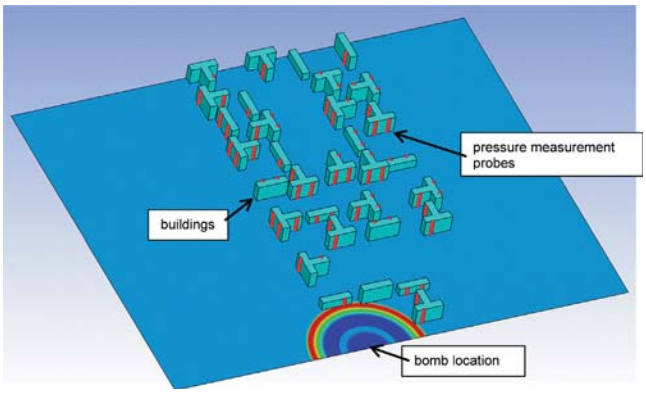

Fig. 17. Simulation setup showing the bomb (bottom), buildings and pressure measurement probe locations (red). (For interpretation of the references to color in this figure legend, the reader is referred to the web version of the article.)

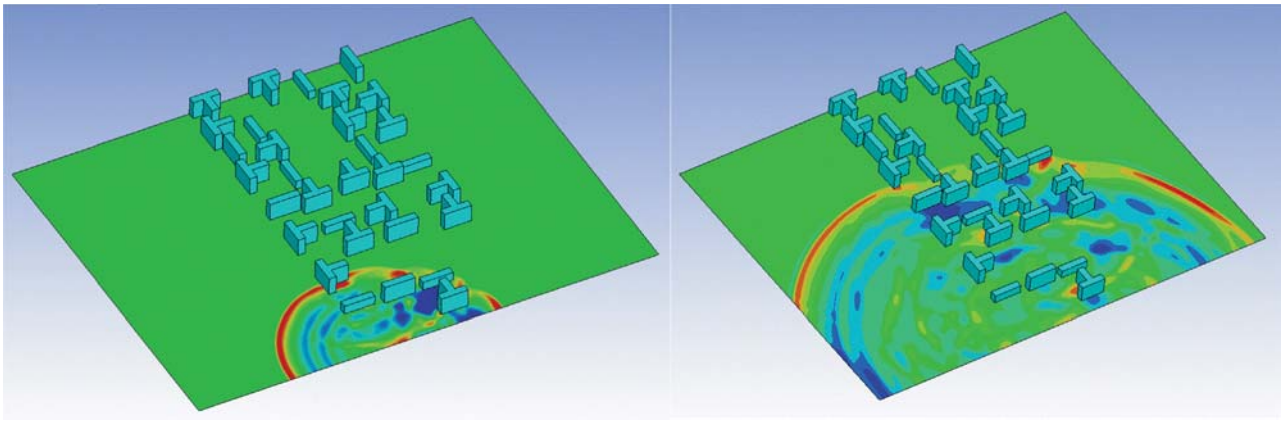

Fig. 18. Pressure contours for the 13,600 kg simulation at 220 ms (top) and 820 ms (bottom).

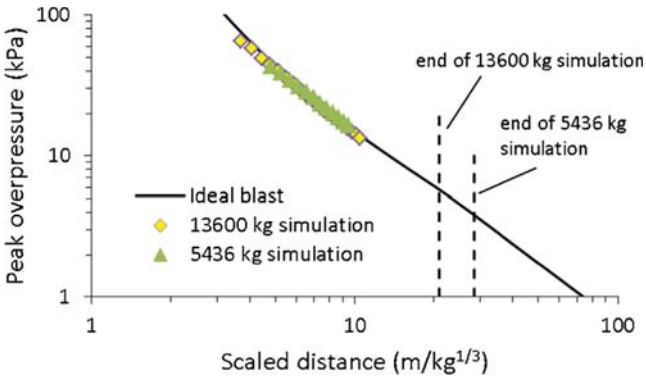

Fig. 19. Peak overpressure as a function of scaled distance ($R/M^{1/3}$). Comparison between simulation and hemispherical surface burst (“ideal blast”).

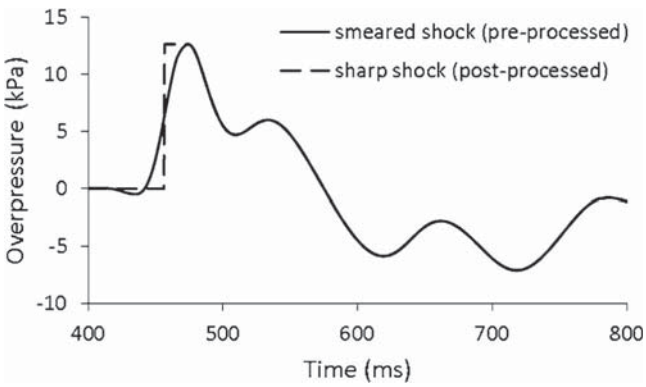

Fig. 20. Post-processing of the shock profile.

The pressure contours for the 13,600 kg simulation are presented in Fig. 18 at two instances showing the effect of the buildings on the shock front and on the flow pattern behind it.

It has been verified that for this cell size the loss of accuracy for the overpressure and impulse due to numerical dispersion (an unwanted artefact) is at most about 10%. This is illustrated in Fig. 19, where the peak overpressure obtained in an unobstructed direction in the simulation is plotted together with the peak overpressure from a hemispherical surface burst [9,20].

Besides this, perhaps, limited deviation, the sharp shock front tends to smear out. The discontinuous nature of a shock is, however, essential for window breakage. Windows are more vulnerable to sharp shock fronts than to pressure waves with a rise time that is larger than the window’s natural period of vibration.

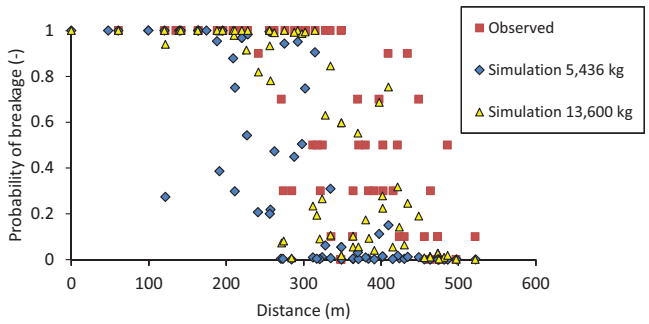

Fig. 21. Comparison between the observed breakage probability and the simulations for 5,436 kg and 13,600 kg.

For this reason, the pressure time signals recorded on the façades were post-processed as in Fig. 20, by keeping the peak overpressure and impulse of the positive phase the same as the pre-processed profile.

For each façade, an average probability of window breakage has been calculated. Fig. 21 presents the results for the 5436 kg and 13,600 kg simulations, as well as the observed probability of window breakage.

As expected, the 13,600 kg simulation consistently shows higher probabilities compared to the 5436 kg simulation. The 13,600 kg simulation shows a much better agreement with the observed breakage probability. A striking feature is that the scatter in the observations is significantly larger than in the simulations. Further variation of the charge mass or the inclusion of the building closest to the bomb location could lead to an even better charge mass prediction (i.e. with a smaller difference with the observed breakage probabilities). This has, however, not been conducted in the current study.

5. Conclusions

The Inverse Explosion Analysis (IEA) tool was developed to estimate the TNT equivalent charge mass and point of origin based on observed damage around an explosion. A statistical method has been developed to combine various types of data, and to determine an overall charge mass distribution. In this paper, inverse models have been presented for two frequently occurring and reliable sources of information: window breakage and building damage. The models have been verified by applying them to the Enschede firework disaster and the Khobar tower attack.

Closest to the explosion, buildings with the highest damage level and façades of which all windows are broken lead to lower bound charge mass predictions. Further from the explosion,

undamaged buildings and façades without window breakage lead to upper bound predictions. The most valuable data comes from the intermediate region.

In relatively open environments, like for the Enschede firework disaster, the models generate realistic charge masses that are consistent with values found in forensic literature. The spread predicted by the IEA tool is however larger than presented in the literature for these specific cases. This is also realistic due to the large inherent uncertainties in a forensic analysis. The IEA models give a reasonable first order estimate of the charge mass in a densely built urban environment, such as for the Khobar tower attack. Due to blast shielding effects which are not taken into account in the IEA tool, this is usually an under prediction. To obtain more accurate predictions, the application of Computational Fluid Dynamics (CFD) simulations is advised.

The TNO IEA tool gives unique possibilities to inversely calculate the TNT equivalent charge mass based on a large variety of explosion effects and observations. The IEA tool enables forensic analysts, also those who are not deep experts on explosion effects, to perform an analysis with a largely reduced effort.

Acknowledgment

The research leading to these results has received funding from the European Community's Seventh Framework Programme (FP7/2007-2013) under grant agreement no. 284585.

References

[1] J.T. Thurman, Practical Bomb Scene Investigation, 2nd ed., Taylor and Francis Group LLC, 2011.
[2] A. Beveridge, Forensic Investigation of Explosions, 2nd ed., CRC Press Taylor and Francis Group, 2012, , ISBN: 978-1-4200-8725-3.
[3] National Institute of Justice, US Department of Justice, A guide for explosion and bombing scene investigation Research Report. https://www.ncjrs.gov/pdffiles1/nij/181869.pdf.
[4] N.F. Scilly, W.G. High, The blast effects of explosions, in: 85th Int. Symp. Loss Prevention in the Process Industries, vol. 1, Cannes, 15–19 September, (1986), p. 39.
[5] P.D. Stone, J. Henderson, World War II bomb damage, accidental explosions and the basis of our current quantity distances, in: 32nd Explosives Safety Seminar, 2006.
[6] S.M. Gilbert, F.P. Lees, N.F. Scilly, A model for hazard assessment of the explosion of an explosives vehicle in a built-up area, in: 26th DoD Explosives Safety Seminar, Miami (pap12c1.pdf), 1994.
[7] D.E. Jarrett, Derivation of the British explosives safety distances, Ann. N. Y. Acad. Sci. 152 (1968) 18–35.
[8] TM 5-13000, Structures to Resist the Effects of Accidental Explosions, Departments of the Army, the Navy, and the Air Force, TM 5-1300, NAVFAC P-397, AFR 88-22, Washington, DC, 1990, November(Superseded by: UFC 3-340-02 Structuresto Resist the Effects of Accidental Explosions, 2008).
[9] C.N. Kingery, G. Bulmash, Airblast parameters from TNT spherical air burst and hemispherical surface burst, Ballistic Research Laboratory, Technical Report ARBRL-TR-02555, Aberdeen, MD, 1984, April.
[10] A. Agresti, B.A. Coull, Approximate is better than 'exact' for interval estimation of binomial proportions, Am. Stat. 52 (1998) 119–126.
[11] S.O. Christensen, Ø.J.S. Hjort, Back Calculation of the Oslo Bombing on July 22nd, using window breakage, in: NDEA, MABS symposium, 2012.
[12] J. Weerheijm, R.M.M. Van Wees, P.C.A.M. de Bruyn, J.W. Karelse, The fireworks disaster in Enschede, Part 1: Overview and reconstruction, in: DoD Explosives Safety Seminar, 2002.
[13] J. Weerheijm, R.M.M. Van Wees, P.C.A.M. de Bruyn, J.W. Karelse, The fireworks disaster in Enschede, Part 2: Safety & pyrotechnics, in: ISEM, Japan, 2002.
[14] J. Weerheijm, R.M.M. Van Wees, J.C.A.M. Van Doormaal, M.P.M. Rhijnsburger, De explosies bij S.E. Fireworks. Deel 1: de kracht van de explosies op basis van waargenomen schade, in: PML 2000-C120, 2000, January.
[15] F.D. Spence, The Khobar Towers Bombing Incident, Staff Report National Security Committee House, 1996, August 14.
[16] D. Thompson, S. Brown, S. Mallonee, D. Sunshine, Fatal and non-fatal injuries among U.S. Air Force personnel resulting from the terrorist bombimg of the Khobar Towers, J Trauma 57 ((2) August) (2004) 208–215.
[17] Special Weapon Agency (DSWA), Report of Khobar Towers Bomb Damage Survey, 1996, July.
[18] P.D. Jamieson, Khobar Towers Tragedy Response Air Force History and Museums Program, United States Air Force, Washington, DC, 2008.
[19] C.J. Hayhurst, R.A. Clegg, M.S. Cowler, New Models and Hydrocodes for Shock Wave Processes in Condensed Matter, Edinburgh, 2002.
[20] AASTP-4, Allied Ammunition Storage and Transport Publication, Manual on Explosives Safety Risk Analysis, 1st ed. Change 2, NATO International Staff, Defence Investment Division, 2008 November.
[21] M.M. van der Voort, R.M.M. van Wees, S.D. Brouwer, M.J. van der Jagt-Deutekom, J. Verreault, A structured approach to forensic analysis of explosions: the TNO Inverse Explosion Analysis tool, in: To be presented at the 5th DAPS conference, Singapore, 19–21 May, 2015.